Combined Action of Gas Radiation and Airfoil Shaped Ribs in Improvement of Solar Heater Performance

S. A. Gandjalikhan Nassab*

Department of Mechanical Engineering, Shahid Bahonar University of Kerman, Kerman, Iran

ABSTRACT: A novel design of solar air heater is proposed in this paper based on the simultaneous exploitation of radiating gas and also airfoil-shaped ribs. Using participating gases with high radiative characteristics concerning the usual working gas, namely air, could show a more promising improvement in thermal performance, especially while this technique is combined with extending surface area. This new concept is demonstrated by simultaneous solution of the radiative transfer equation considering both the diffuse and collimated beams coupled with momentum, energy, and continuity equations. The set of governing equations are solved using the finite element method in a steady-state condition by the COMSOL Multi-physics. The well-known $\kappa - \varepsilon$ model is used in calculations of turbulent stress and heat flux in numerical simulation. Through the presented results, radiative gas proved its full potential to serve as a future working gas in solar gas heaters. Its combination with the airfoil-shaped ribs shows magnificent 88% thermal efficiency and gas outlet temperature up to 85°C in the test cases. The contributions of airfoil-shaped ribs and also the gas radiation to increase thermal performance are computed equal to 7% and 66%, respectively.

1- Introduction

According to the World Energy Council's scenario for 2050, energy efficiency is crucial in dealing with demand outstripping supply. Consequently, it should be a part of researchers' mission to facilitate Renewable Energy (RE) as an essential pillar for sustainable development and make it as efficient as possible. A Solar Air Heater (SAH), in its general form, is an inexpensive heat exchanger for converting solar radiative heat flux into air enthalpy, which may be used as a heating system [1, 2]. As an important RE facility, SAH covers wide applications from cooking, drying agricultural products, providing the required energy for air conditioning systems, etc. [3, 4]. SAHs have different types and configurations and the working mechanism is divided into two classes of natural and forced heaters as the former required no external source for fluid flow while the latter uses a blower or induced fan for fluid motion. Consequently, the forced SAH is relatively expensive and used where a higher and tunable flow rate is required, while natural SAH is cheaper and simpler. For the forced SAH, there is a possibility to be employed in a closed-loop thermal-solar system. The advantage of using a closed-loop system is that there are more options for the better-working gas to be selected rather than air.

Due to its outstanding feature, SAH is a popular renewable facility. It is economically affordable, has a simple configuration for installation, requires less care for commissioning, and can also considerably decreases the expense of

*Corresponding author's email: ganj110@uak.ac.ir

energy consumption wherever it is involved [5]. However, its low thermal performance due to the low thermal conductivity of working-gas, and low-speed thick-boundary layer, making this renewable facility less attractive. The currently available commercial SAHs, have not been widely employed in many applications because they cannot meet the required temperature set point. Also, in some cases, its efficiency cannot even justify the low initial expenses regarding its installation and commissioning, and regular maintenance. Several numerical and experimental scientific works have been published just to attack this issue and propose a new solution to enhance SAH's thermal performance. The ideas include convex and concave channels for different curvature radii [6], serpentine wavy wire-mesh packed bed [7], an internal multiple-fin array in the direction of airflow [8] as well as a new geometry of arched absorber [9]. The concept of extruded surfaces in many types and geometries for heat transfer enhancement also has been addressed by some investigations [10]. A critical review of the ribbed solar air heater was presented in the paper by Nidhul et al. [11]. In that study, a three dimensional Computational Fluid Dynamics (CFD) analysis was carried out to investigate the effect of V-rib type on the performance of SAHs. Also, the energy and exergy analyses were done to determine the first law and exergetic efficiencies. Numerical findings revealed 31.6% higher exergetic efficiency in the case of using multiple V-ribs with a gap in the construction of a solar air heater. Numerical analysis of a plane SAH with a perforated circular absorber plate was carried out by Shetty

et al. [12]. In that research work, an attempt was made] to investigate the performsance improvement due to the elimination of laminar viscous layer because of using the perforable absorber plate. The numerical analysis based on the CFD technique was conducted for Reynolds numbers ranging from 3000 to 21,000. The average increase in the thermal efficiency of 23.33% was obtained for the configuration with 8 mm diameter vents and 36 number of vents compared to the base model without the perforable absorber plate.

The thermo-hydraulic characteristics of a SAH with quarter-circular ribs on the absorber plate were studied numerically by Mahanand and Senapati [13]. A comparison of the three different arrangements of the quarter-circular ribs was performed. The ribs were aligned periodically in a transverse manner to the convection airflow. The numerical simulation of the flow equations were carried out for a two-dimensional computational domain using the finite volume multi-grid solver of ANSYS-Fluent-18. The impact of relative roughness pitch and Reynolds number on the thermo-hydraulic performance of the ribbed solar air heater was analyzed in that study and the optimized rib geometry in the investigated range of parameters was determined. It was found that the SAH with quarter-circular ribs having a relative roughness pitch of 7.14 delivers a maximal thermal enhancement ratio (representing the overall energy performance) of 1.88 in the studied parametric range.

As seen, all of the abovementioned cases are valuable attempts to improve the performance through the creation of changes in the SAH configuration. After surveying extensive review studies in this area, it is found that very few research studies have addressed performance enhancement of any kind of SAH through the proposed methodology of this study. Almost all experimental works dealt with solar air heaters in which air as a poor-radiative gas was used. Consequently, the inherent thermal characteristics of radiating gases have been ignored in calculations and practical applications. As seen, all mentioned methods belong to the same group of heat transfer enhancement from the thermodynamic point of view. For those applications in which air is not mandatory to be used, using a working gas with higher radiative properties, such as pressurized CO2, can satisfy the requirements and provide high-temperature flow at its outlet section without essential change of configuration. A few recent research studies on Solar Gas Heaters (SGH) addressed this concept. Dehghani and Gandjalikhan Nassab [14] studied the gas radiation effect in laminar flow within single and double planar SGH. They showed that the efficiency of double-flow gas heaters is higher than that of single-pass types and this behavior is enhanced by gas radiation. The radiating effect of working gas instead of air on the thermal performance of SGH with the laminar flow was investigated by Frouzan Nia et al. [15]. It was revealed that the outlet temperature would increase at high optical thicknesses, and a more uniform temperature distribution occurs across the SGH channel.

In the case of volumetric radiation, the boundary surfaces and their role in absorbing and emitting radiative beam are very important, such that extending surface area enhances the radiative heat transfer as well as its convection counterpart. This fact motivates the author to conduct a theoretical investigation on radiative gas potential and the method of extending the surface area to change the destiny of solar heaters and to receive more attention from industries. Also, using the airfoil-shaped ribs on the absorber surface of solar heaters that leads to less pressure drop has not been reported up to now. To materialize this aim, the current study introduced radiating gas into a plane SGH with airfoil-shaped ribs and presented a comprehensive thermo hydrodynamic analysis of steady-state turbulent forced convection to show its advantages. Because of the gas radiation, the differential radiative transfer equation (RTE) will also be added to the conventional coupled nonlinear governing equations and makes it even more complicated. From this complexity, a peculiar practical result will be extracted and presented quantitatively. It should be recalled that as the system must be charged with an appropriate radiating working gas such as carbon dioxide, a closed-loop should be designed for the proposed SGH. An example of the application is shown in Fig. 1, which is about a closed-loop solar system with thermal storage for space heating.

2- Model Description

A schematic of the plane SGH which is considered a non-concentrating stationary collector for converting solar radiation into gas enthalpy with its attached ribs is shown in Fig. 2. In order to capture all the important factors influencing the SGH performance and provide reliable results, all the components consist of the glass cover, absorber plate, and insulation are included in the simulation.

Due to the support of pressure gradient by an induced fan, the gas flow enters from the inlet section, and the forced convection heat transfer takes place with the absorber. The Reynolds number value based on the average inlet velocity of 1 m/s used in all simulations becomes $\rho \bar{V} D_h / \mu = 4100$, which corresponds to turbulent flow. A great part of the total incoming solar radiation, transmitted from the glass cover and the gas layer, is absorbed by the absorber plate and the radiating gas flow directly absorbs a portion of solar radiation. The airfoil-shaped ribs attached to the absorber plate increase the surface area in both radiation and convection mechanisms, and its mixing effect breaks the thermal boundary layer. Each of the ribs has the profile of symmetric airfoil NACA0012 to have low-pressure drop and avoid separation. In the numerical simulation, the length of SGH is equal to L, the chord of the applied airfoil is c, and the air gap thickness is denoted by b. The outer surfaces of SGH are exposed to convection and radiation with the surroundings. The equivalent convection coefficient h_{eq}, is used for considering combining convection and surface radiation on these boundary surfaces.

All thermophysical properties of the pure-absorbing radiative working fluid, which is considered incompressible Newtonian ideal gas, are provided in Table 1. As the solution is non-isothermal with large temperature variation in the computational domain, the gas properties are considered temperature dependent. It should be noted that the reported values in Table 1 were set at the temperature of the inlet section.
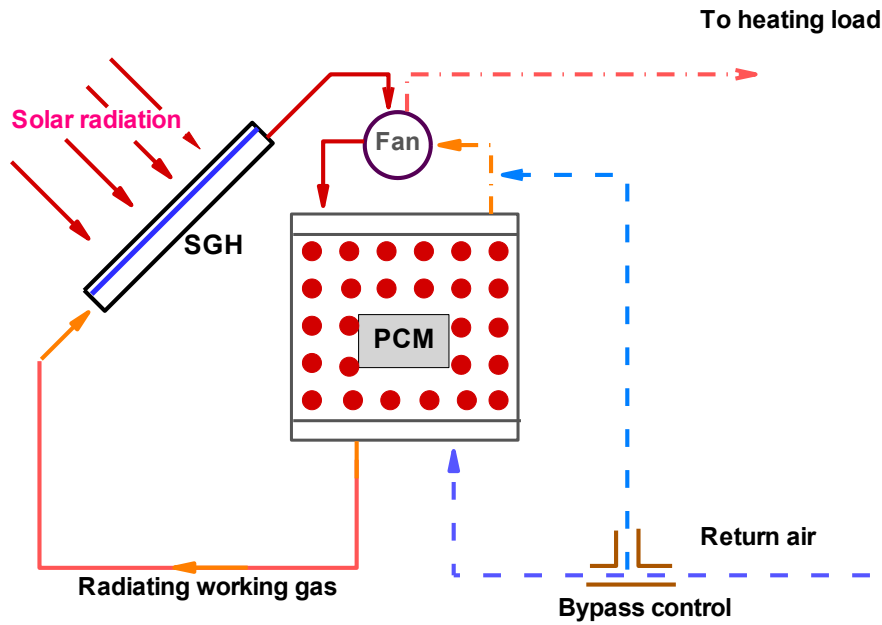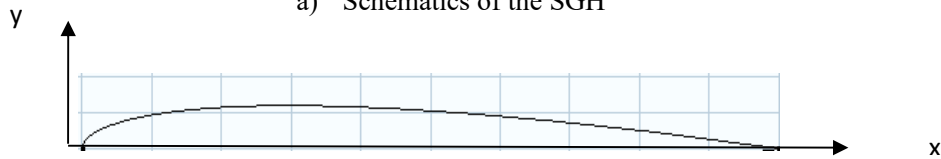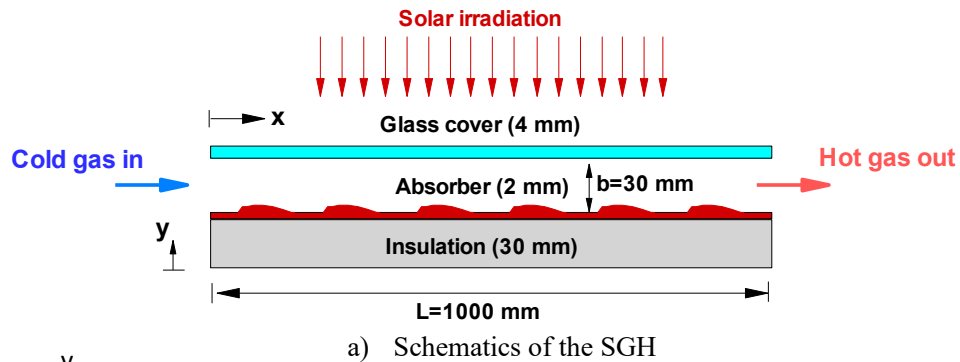
Fig. 1. An application of SGH for space heating with thermal storage

a)   Schematics of the SGH

$$y = 0.595c \times [\, 0.298\sqrt{(x\,/\,c)} - 0.127(x\,/\,c) - 0.358(x\,/\,c)^{2} + 0.292(x\,/\,c)^{3} - 0.105(x\,/\,c)^{4}\,]$$

b)   The geometry of airfoil (NACA0012)

Fig. 2. Geometry and dimensions of SGH

In Table 2, the dimensions and physical properties of solid elements, including the glass cover, absorber, and insulation, are provided. Along with the absorber, six airfoil-shaped ribs with a chord of c=10 cm, whose profiles and geometrical fac-tors are depicted in Fig. 2, are used for heat transfer augmentation. The first rib is located at x=8 cm, while the distance between the ribs is c/2.

Table 1. Radiative gas information and characteristics

T_{in} [K]	V_{in} [m/s]	P_{out} [Pa]	σ_s [1/m]	σ_a [1/m]
293	1	0	0	0, 1, 5, 10
C_p [J/kg.K]	k [W/m.K]	ρ [kg/m³]	μ [Pa.s]	**Inlet turbulent intensity**
1000	0.026	1.22	1.8×10^{-5}	5%

Table 2. Physical properties of solid materials

Physical properties	Insulation	Glass cover	Absorber
Length [m]	1	1	1
Thickness[mm]	30	4	2
Thermal conductivity [W/m.K]	0.037	0.78	400
Surface emissivity	_	0.9	0.95
Reflectivity	_	0.05	0.05

Table 3. Summary of methodology and values of constants

Flow regime	Flow modeling	Algorithm	Convection type	Reynolds No.
Turbulent	Standard $k - \varepsilon$	SIMPLE	Forced	4.1×10^3
C_1	C_2	C_3	σ_ϵ	σ_k
1.44	1.92	0.09	1.3	1.0

3- Theory

In the modeling and simulation of solar heater, the governing equations, including the conduction equation for all solid elements and conservation laws for turbulent forced convection flow in their Reynolds averaged form, were solved by the Finite Element Method (FEM). The set of governing equations for steady-state incompressible turbulent forced convection flow based on the standard method [16] can be stated as follows.

$$\nabla.V = 0 \tag{1}$$

$$\frac{D(\rho V)}{Dt} = -\nabla p + \nabla.[(\mu + \mu_t)(\nabla V + \nabla V^T)] \tag{2}$$

$$\frac{D(\rho C_p T)}{Dt} = \nabla.[(k_{th} + \frac{C_p}{\text{Pr}_t})\nabla T] + \nabla.q_r \tag{3}$$

$$\frac{D(\rho k)}{Dt} = \nabla.[(\mu + \frac{\mu_t}{\sigma_k})\nabla k] + P_k - \rho\varepsilon + S_k \tag{4}$$

$$\frac{D(\rho\varepsilon)}{Dt} = \nabla.[(\mu + \frac{\mu_t}{\sigma_\varepsilon})\nabla\varepsilon] + C_1\frac{\varepsilon}{k}P_k - C_2\frac{\rho\varepsilon^2}{k} + S_\varepsilon \tag{5}$$

More details are provided in Ref. [17] and also in Table 3. The numerical procedure and the algorithm of the solution In addition, the conduction equations were also solved for temperature computation in solid elements, namely glass cover, absorber, and insulation layer. Because of the glass cover radiative absorption, the conduction equation for this part of the heater contains a source term. The present coupled heat transfer is known as conjugate one, at which the continuity of temperature and heat flux must be imposed at the gas-solid interfaces.

Because of the radiative source term in the gas energy equation, the RTE was solved by the Discrete Ordinate Method (DOM) for the computation of radiation intensity inside the participating gas flow.

3- 1- Gas radiation modeling

All terms in the governing equations were introduced in the previous section except : $\nabla.q_r$, in the gas energy equation that stands for the gas radiation effect. This term usually has been neglected due to the very low radiative properties of working gas in the analysis of solar air heaters. In the present numerical simulation, as the thermal system is charged with radiating gas, the divergence of radiating heat fluxes for the considered participating medium is not dispensable anymore. This term can be computed by [18]:

$$\nabla.q_r = 4\pi\sigma_a I_b - \sigma_a \int_{4\pi} I(r,s)d\Omega \tag{6}$$

The first term denoted the black body radiation intensity, while the second term stands for the incident radiation. The radiation intensity can be computed from the RTE for an absorbing, emitting, and non-scattering gray medium at any direction and position. This differential equation for a pure absorbing-emitting gray medium can be stated as follows [18]:

$$(s.\nabla)I(r,s) = \sigma_a[-I(r,s)+I_b(r)] \tag{7}$$

The solar beam that enters the collector cavity via the glass cover is collimated. To consider the effects of the solar beam in radiation computations, the radiant intensity within the heater is separated into two parts: (1) the remnant of the directional or collimated short wave beam after partial extinction and absorption along its path, and (2) a diffuse part, which is the result of longwave emission from the gray absorber and glass cover surfaces and also from the radiating gas. Thus, we set [18]:

$$I(r,s) = I_c(r,s) + I_d(r,s) \tag{8}$$

Such that the equation governs the collimated beam which is similar to RTE is as follows:

$$(s.\nabla)I_c(r,s) = -\sigma_a I_c(r,s) \tag{9}$$

This equation is subjected to the following boundary condition on the glass-gas interface.

$$I_c(r_w,s) = \tau_{glass}.q_{sun}.\delta(s-s_c(r_w)) \tag{10}$$

The differential Eq. (9) with its boundary condition are readily solved as

$$I_c(r,s) = \tau_{glass}.q_{sun}.\delta(s-s_c(r_w)).e^{-\tau_c} \tag{11}$$

where, $\tau_c = \int_0^s \sigma_a ds$ is the optical thickness and δ is the Dirac-delta function. For the diffusion part of radiant intensity, the following RTE is employed for radiation computation [18].

$$(s.\nabla)I_d(r,s) = \sigma_a[I_b(r) - I_d(r,s)] \tag{12}$$

The radiative boundary condition for the above equation depends on whether the surfaces are semitransparent or opaque. For the opaque boundary surfaces, it will be as follows:

$$I_d(r_w,s) = \varepsilon_w I_b(r_w) + \frac{1-\varepsilon_w}{\pi} \int_{\vec{n}_w \cdot \vec{s}' \leq 0} I_d(r_w,s)|\vec{n}_w \cdot \vec{s}'|d\Omega'$$
$$\vec{n}_w \cdot \vec{s}' \geq 0 \tag{13}$$

and for the semitransparent one which is the glass cover in the present case, the following boundary condition is considered.

$$I_d(r_w,s) = \varepsilon_w I_b(r_w) + \frac{1-\varepsilon_w}{\pi}[H_c(r_w) + \int_{\vec{n}_w \cdot \vec{s}' \leq 0} I_d(r_w,s)|\vec{n}_w \cdot \vec{s}'|d\Omega' \quad \vec{n}_w \cdot \vec{s}' \geq 0 \tag{14}$$

Where

$$H_c(r_w) = \int_{n_w \cdot \vec{s}' \leq 0} I_c(r_w,s)|\vec{n}_w \cdot \vec{s}'|d\Omega'$$
$$\vec{n}_w \cdot \vec{s}' \geq 0 \tag{15}$$

According to the DOM, RTE was solved for a set of discretized directions, $\vec{s}_i$, i=1,2,3,…,n; while integrals over solid angle were replaced by the numerical quadrature based on the following relation [18]:

$$\int_{4\pi} f(\vec{s})d\Omega = \sum_{i=1}^{n} w_i f(\vec{s}_i) \tag{16}$$

For the present 2D computational domain, the S4 approximation including twelve discretized directions was employed (n=12).
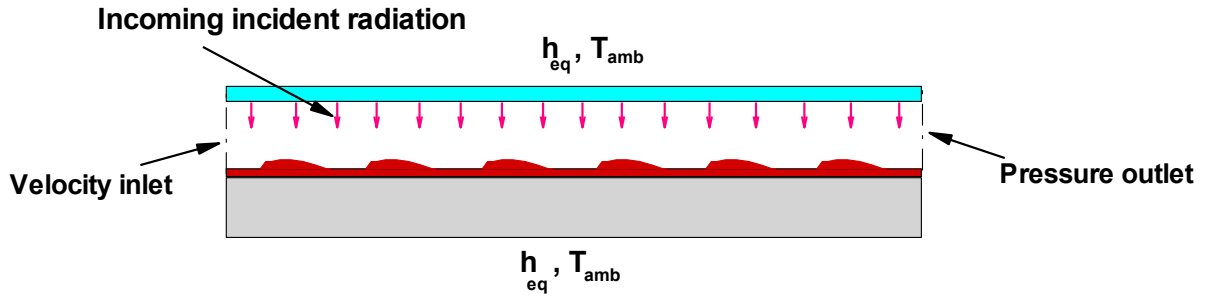
Fig. 3. Schematic diagram of the computational domain and imposed boundary conditions

3- 2- Boundary condition

The following boundary conditions were imposed in the numerical solution of the flow equations:

- The radiative working gas enters into the SGH with the uniform constant temperature $T_{in=}$ 293 K and a fully developed velocity profile with an average velocity of 1m/s.
- Zero gauge pressure is considered at the outlet.
- No-slip condition for all solid walls is employed.
- Zero axial gradients are employed at the outlet for all dependent variables.
- In radiation computation, a constant radiative intensity due to an incoming solar collimated beam normal to the glass surface corresponds to the heat flux $1000 \times \tau_{glass}$ (W/m²) is imposed on the gas-glass interface. The glass transmissivity can be computed as $\tau_{glass} = 1 - \rho_{glass} - \alpha_{glass} = = 0.05$, based on the value of 0.05 for glass reflectivity.
- The continuity of temperature and heat flux at the gas-solid interface are also imposed, wherein the radiating gas, the total heat flux is the sum of conductive and radiative terms as follows:

$$[-k_{th} \frac{\partial T}{\partial n}]_{solid} = [-k_{th} \frac{\partial T}{\partial n}]_{gas} +$$
$$\varepsilon_w [\pi I_b(\vec{r}_w) - \sum_{\vec{n}_w \vec{s}' \leq 0} w_i |\vec{n}_w \vec{s}'| I((\vec{r}_w)] \tag{17-a}$$

$$T_{solid} = T_{gas} \tag{17-b}$$

- The convection boundary condition with its equivalent convection coefficient on the glass surface and insulation adjacent to the surrounding is employed. The convective and radiative parts of the equivalent coefficient of heat transfer are calculated based on the following expressions [19]:

$$h_{conv} = 5.7 + 3.8 V_{wind} \tag{18}$$

$$h_{rad} = \sigma \varepsilon_g \frac{(T_g^4 - T_{sky}^4)}{T_g - T_{amb}} \tag{19}$$

$$T_{sky} = 0.0522 T_{amb}^4 \tag{20}$$

Where

A schematic diagram of the computational domain and the applied boundary conditions is shown in Fig. 3.

3- 3- Grid distribution and grid independence test

The unstructured triangular grid generation method was used for the 2D geometry of SGH because of the ribs on the absorber surface. The grid study is needed to find an optimum number of grid nodes inside the computational domain that makes numerical results reliable and independent from the spatial discretization and simultaneously confers a computationally cost-effective mesh. For this, the maximum values of air temperature, velocity, and turbulent kinetic energy as the most sensitive parameters to the number of nodes were selected for checking the grid independency. The values of these parameters against different grid sizes were computed, and the results are presented in Table 4. As seen, the relative error of sought parameter concerning the previous step goes down as the number of nodes increases. Table 4 shows that the optimum number of elements in the computational domain is 35610, such that the relative error in computing the test parameters falls below 1% when a more refine grid with 53410 elements is considered in the computational domain.

According to the grid study, the unstructured discretized domain with 35610 nodes was used for the 2D geometry of SGH as is depicted in Fig. 4. As seen, near the walls, the mesh was refined to precisely capture the high gradient of dependent variables. As the wall function is used for velocity computation very closed to the solid walls, the minimum size of grid nodes is so chosen for having, $y^+ \geq 30$, which lies out of the buffer zone. In the present discretized computational domain with clustering near walls, the minimum value of y^+ is equal to 34.
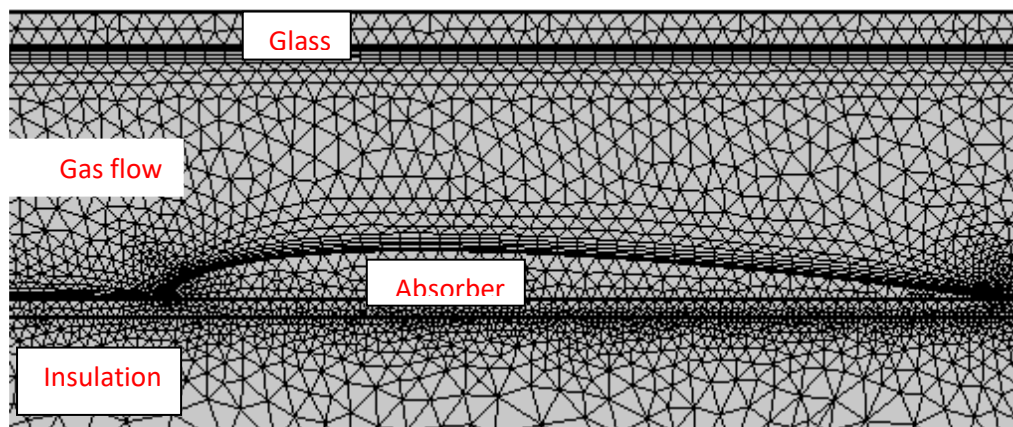
Fig. 4. The triangular unstructured grid nodes in a portion of the computational domain (Zoomed image)
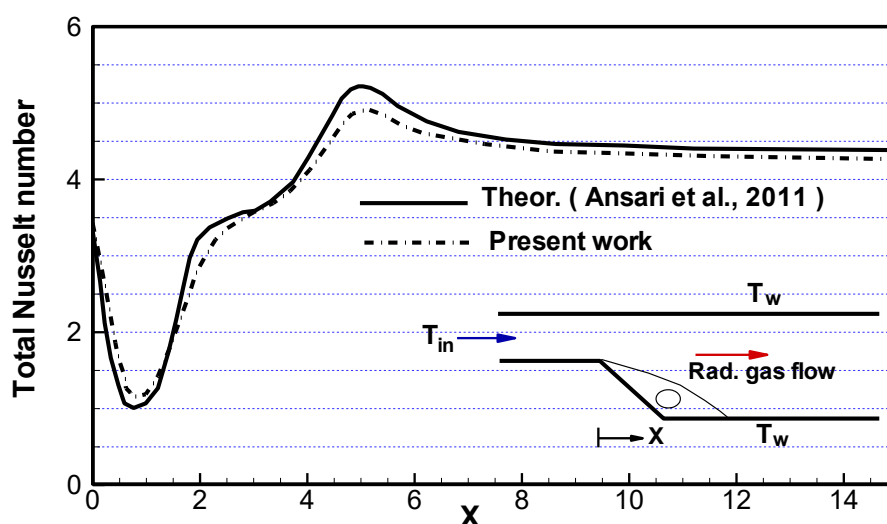

Fig. 5. Comparison of the computed Nusselt number distributions on the lower wall with theoretical results [20]

3- 4- Validation of numerical scheme

The present numerical simulation was validated first with the numerical findings by Ansari and Nassab [20] and then with experimental results reported by Chabane et al. [21]. In Ref. [20], laminar forced convection of radiating gas in a duct with an inclined backward step was simulated numerically. In that study, the set of governing equations, including conservations of mass, momentum, and energy, was solved by the finite volume method using the blocked-off technique. The radiation computations were based on the solution of RTE with the DOM. The distribution of the Nusselt number, which is the sum of convective and radiative parts, is plotted in Fig. 5, and a comparison is made with the present theoretical results. As seen, the trend and value of the computed Nusselt number in the present work are closed to those reported in Ref. [20]. This consistency can validate the present convection and radiation computations.

For further verifying the accuracy of the present analysis, the plane solar air heater which was investigated experimentally by Chabane et al. [21] is numerically simulated, and the findings are compared with experimental data. The analyzed SAH is exactly similar to what it is in the present work but without any ribs on the absorber plate and with different geometrical dimensions. At two different air mass flow rates, the SAH efficiency is calculated during the sunny day of the experiment, and its distributions are plotted and compared with an experiment in Fig. 6. This figure illustrates that the thermal efficiency increases with an increase in air mass flow rate, and the maximum value of this parameter takes place at 1 PM. However, there is a good consistency between the present numerical findings with the experiment. It should be mentioned that in this test case, the working gas was considered as a nonparticipating medium due to the very low radiative effect of airflow ($\sigma_a = 0$).
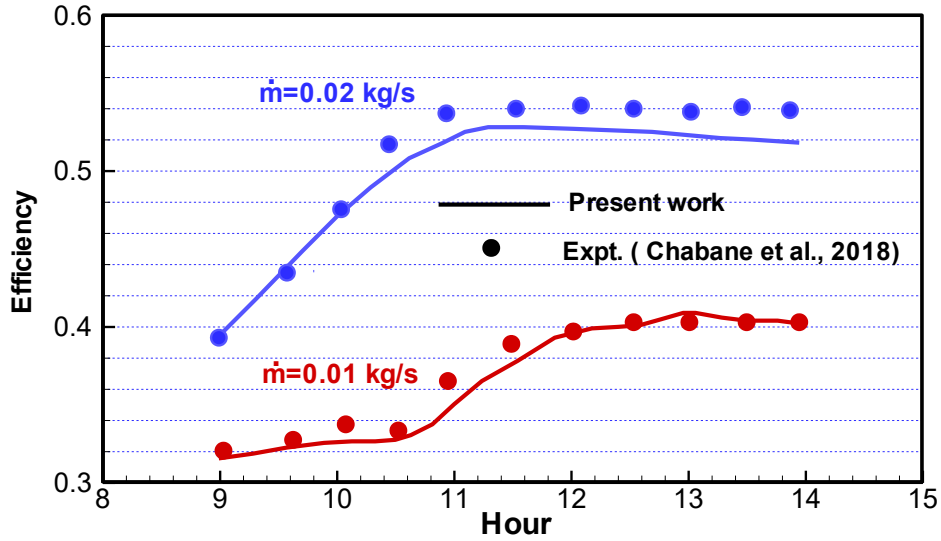
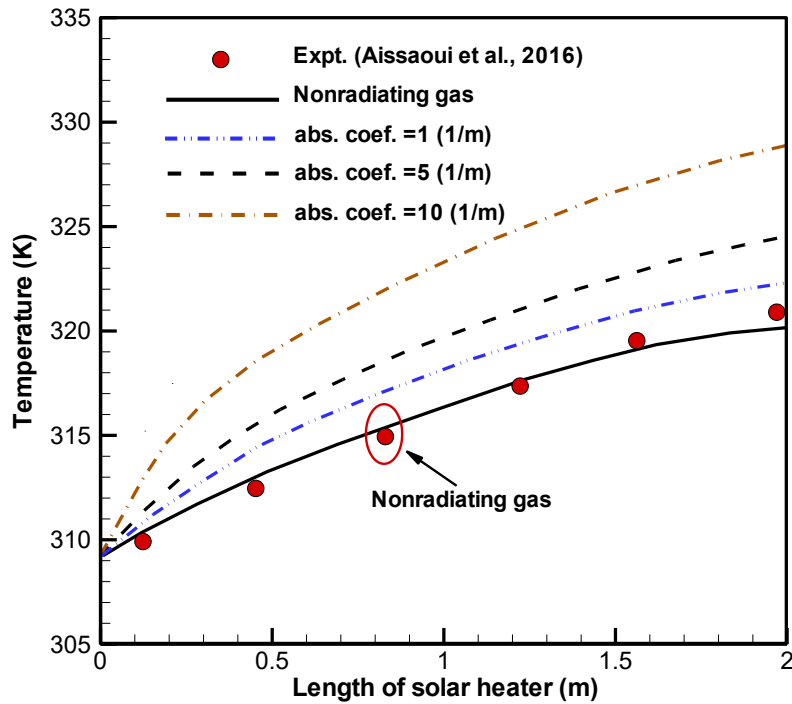**Fig. 6. Comparison of the computed thermal efficiency with experimental data [21]**

Fig. 7. Gas temperature variation along the heater and comparison with experimental data [22],
Re=3.84×10⁴,q_sun=700 W/m²

In the third test case, the plane solar air heater which was analyzed both theoretically and experimentally by Aissaoui et al. [22] was simulated for validation. The SHA in that study is similar to the present simulated clean solar heater (without ribs). Different values of the gas absorption coefficients including the non-radiating case were considered in the simulation and the variations of gas flow along the heater are drawn in Fig. 7 in comparison to the experimental data reported in Ref. [22] for airflow. It should be mentioned that the comparison was made only for the zero value of the gas absorption coefficient,t as the working gas (air) is non-radiating. Fig. 7 reveals an increasing trend for the gas temperature along the heater, such that the rate of gas temperature increase gets higher values for more radiating gas flows. Satisfactory qualitative and quantitative agreement is seen between the present numerical findings and experimental data.
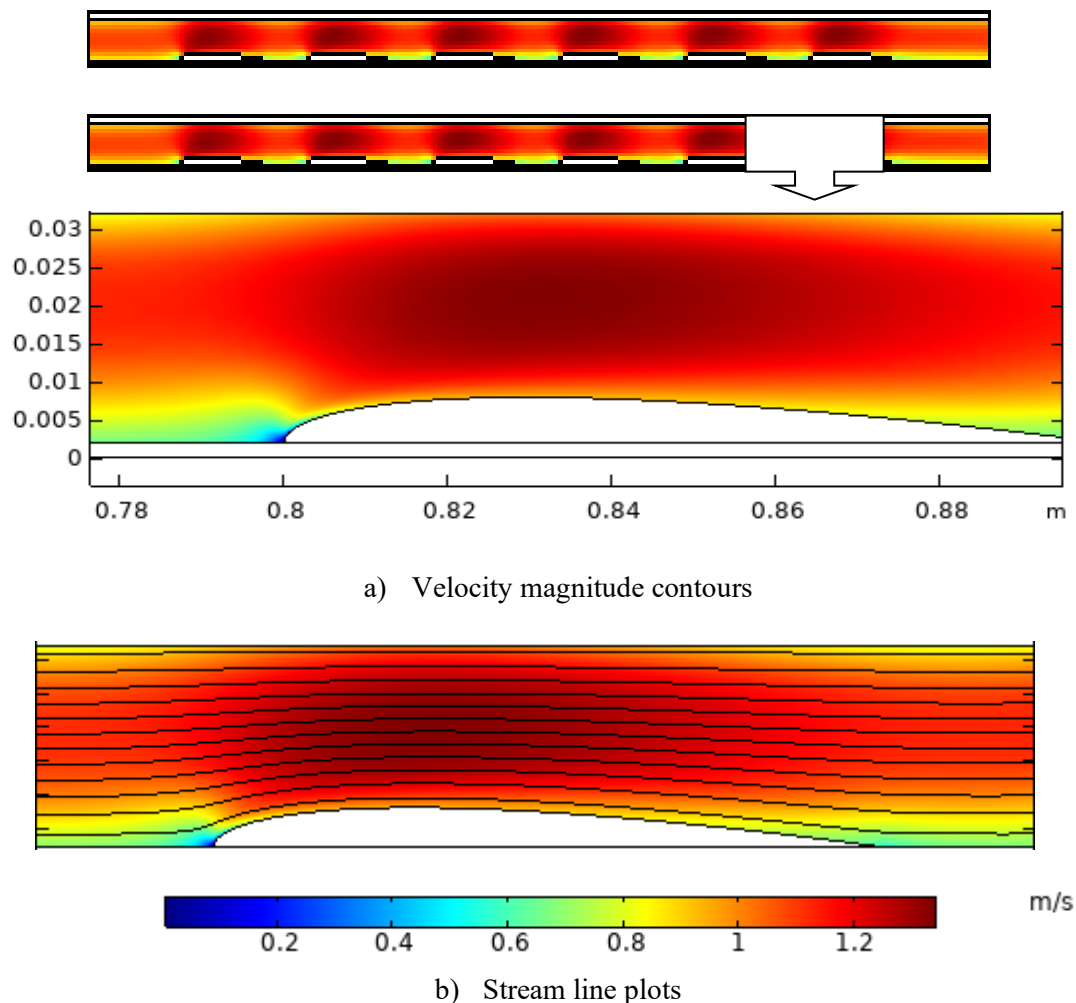
a)   Velocity magnitude contours

b)   Stream line plots

Fig. 8. Vlocity magnitude contours and streamlines in turbulent convection gas flow inside the SGH

4- Results and Discussion

After validation of the numerical procedure, from the grid generation to the model adoption and convergency, numerical simulations in steady-state turbulent forced convection of radiating gas in a planar SGH at the presence of airfoil-shaped ribs are presented in this section.

In Fig. 8, the hydrodynamic characteristics of the gas flow field are discussed by plotting the contour of velocity magnitude. The zoomed view of the velocity field and also streamlines are provided for better demonstration. The effect of attached ribs can be seen easily, such that the gas velocity increases as it passes from each of the airfoil bodies such that the ribs act as nozzles to accelerate the flow locally. This behavior augments the heat transfer rate from the absorber surface to the core of cold gas flow. As an important finding, one can recall that there is not any recirculated domain down-

stream of the ribs, which is known as a low heat transfer zone. This phenomenon is seen in the streamline plot downstream of the rib.

In Fig. 9, the pressure contours in the duct of SGH are plotted. As the convective gas flow passes over each airfoil which provides positive and negative accelerations in the axial direction, similar to flow in the converging-diverging nozzle, the gas pressure varies along with the heater with a wavy form distribution as seen in Fig. 9. The distribution of gas pressure along the duct mid-line shown in Fig. 10 also reveals the wavy form of gas pressure variation.

As the working gas has a radiative effect, before discussing the thermal behavior, it is first required to illustrate the incident radiation distribution clearly. A study about this parameter will then help us better interpret temperature distribution within the SGH.
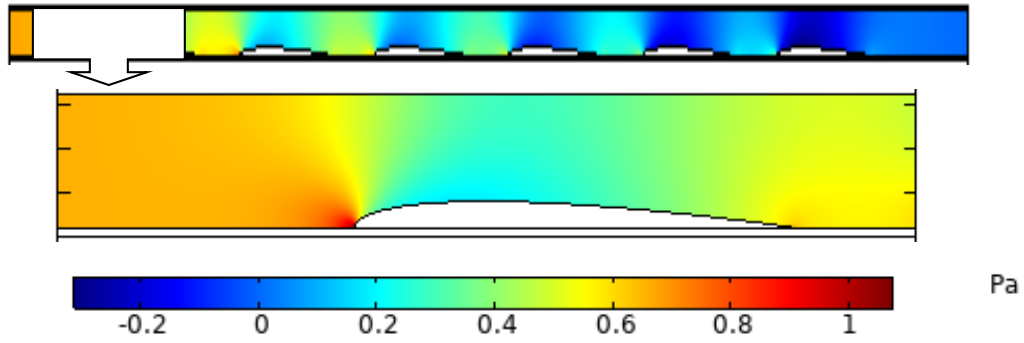
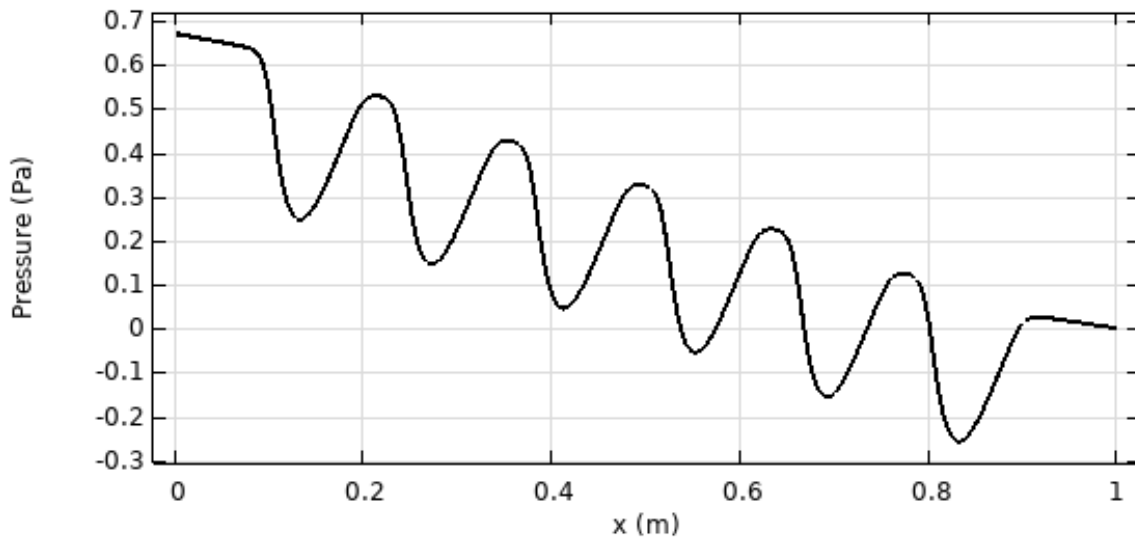**Fig. 9. Pressure contours inside the duct of SGH**

**Fig. 10. Gas pressure variation at the mid-line along the x-direction**

With this short introduction, Fig. 11 shows the distribution of incident radiation, G, within SGH for three different absorption coefficients and non-radiating gas. It is seen that the non-radiating gas does not have any capability of absorbing incident solar radiation. Hence, the intensity of the incoming beam remains fixed across the gas layer. But in the cases of radiating gas, especially with a high absorption coefficient, a decreasing trend is seen for incident radiation by direct absorption of solar heat flux by the participating gas. This behavior is enhanced for the thick medium, $\sigma_a = 10\,\mathrm{m}^{-1}$. . The molecules of gas adjacent to the transparent surface completely dampen the incoming irradiation, and the incoming irradiation is not allowed to penetrate the heater duct. The zoomed view of the incident radiation is also presented for each case for better observation.

Fig. 12 indicates the temperature pattern inside the whole parts of the heater by plotting the isotherms. The maximum temperature happens on the absorber, which is under the incidence of solar heat flux. It is seen that the

thermal energy penetrates from this element towards the insulation layer by pure conduction and into the gas flow by all of the three heat transfer mechanisms. Fig. 12 shows how the convective gas flow is heated as it passes along the duct of the heater by both convection heat transfer via the hot absorber pate and by direct absorption of incoming irradiation from the glass cover. As the ability of working gas in absorbing radiation increases, the temperatures of the absorber and insulation layer get decreasing trends because the more rate of heat transfer happens into the gas flow with the help of the gas radiation effect. This behavior leads to considerable improvement in the SGH performance. If one compares the zoomed isotherm plots in the cases of non-radiating gas and strongly radiating gas ($\sigma_a = 10\,\mathrm{m}^{-1}$), it can be seen that more thermal energy is penetrated from the absorber into the core of convective flow due to radiative heat transfer that leads to the increase of gas outlet temperature. For the SGH application, a higher outlet temperature is always interpreted as better thermal performance.
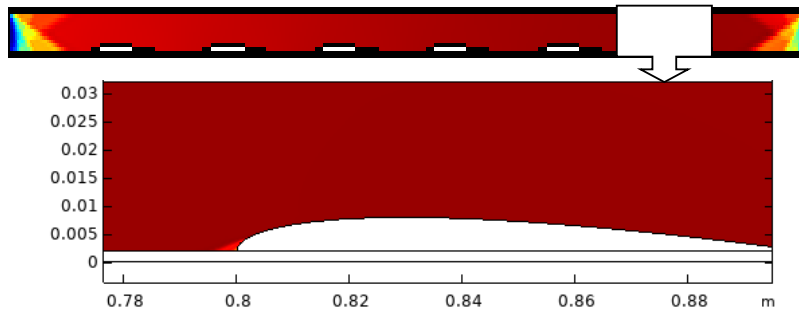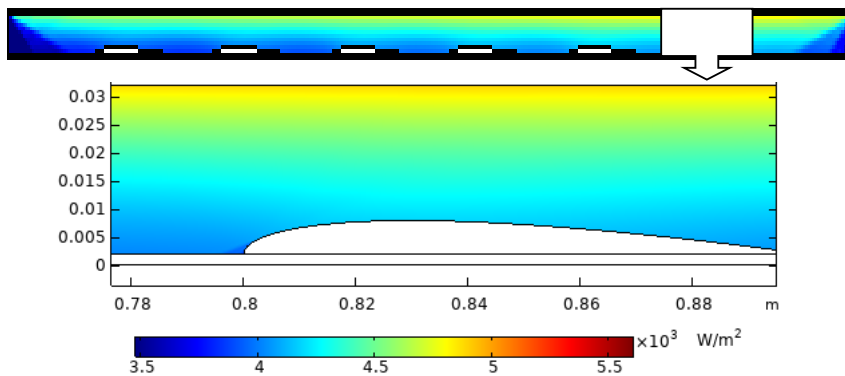
a) Non radiating gas
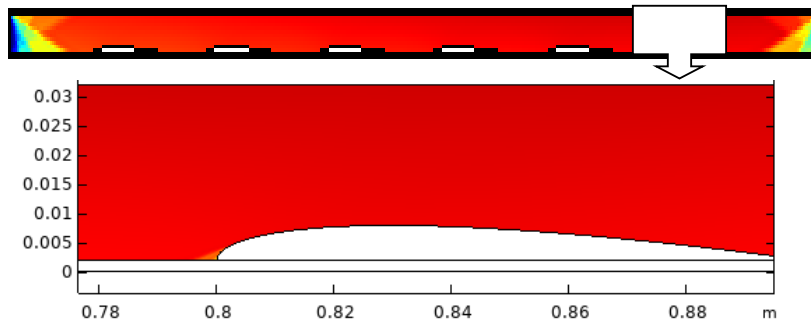
b) $\sigma_a = 1 \text{ m}^{-1}$
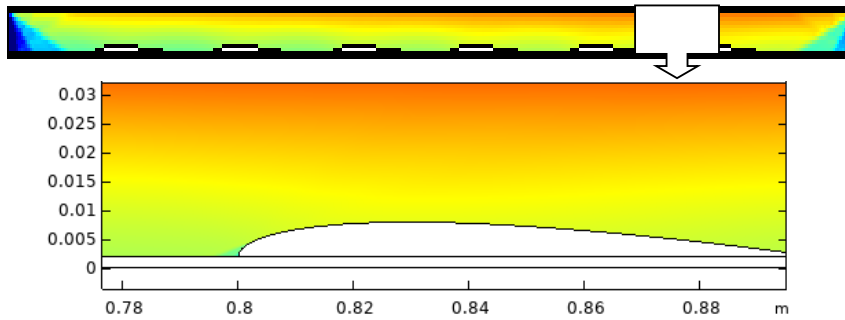
c) $\sigma_a = 5 \text{ m}^{-1}$

d) $\sigma_a = 10 \text{ m}^{-1}$

Fig. 11. The incident radiation contour plots inside the radiating gas flow

303

a) Non radiating gas

b) $\sigma_a = 1 \, m^{-1}$

c) $\sigma_a = 5 \, m^{-1}$
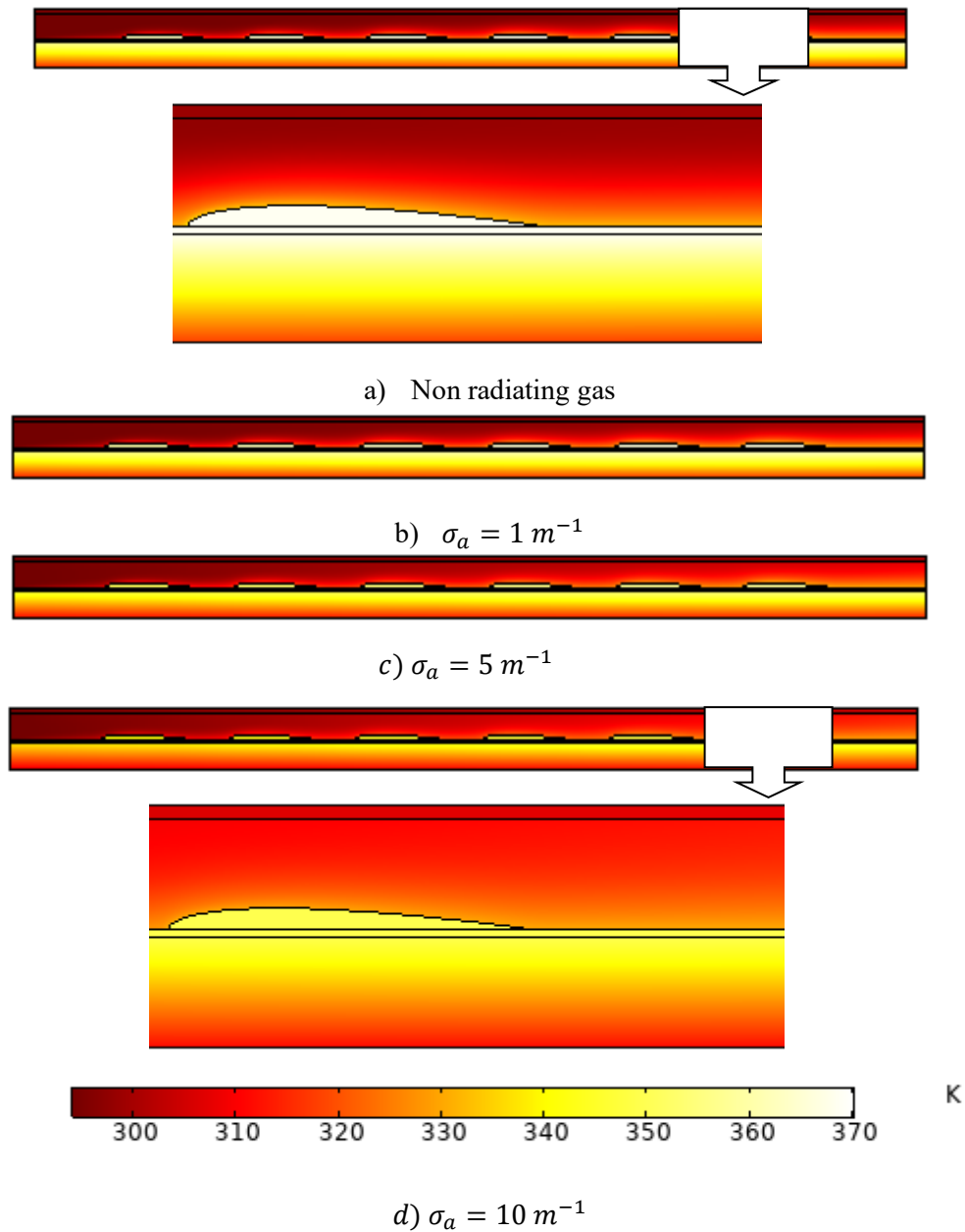
d) $\sigma_a = 10 \, m^{-1}$

Fig. 12. Isotherm plots inside the whole SGH

To demonstrate the thermal behavior of the proposed SGH more, the temperature variations along the y-direction side of the whole parts, including the insulation layer, absorber plate, gas flow, and glass cover, are drawn in Fig. 13 at the axial section x=L/2. This figure can help the readers to have a good image of SGH thermal characteristics. As expected, the maximum temperature belongs to the absorber. It is seen that the minimum value of glass temperature and maximum value of insulation temperature take place for non-radiating gas. In this case, the glass is hotter than the gas flow because of the glass's radiative absorption, and a small part of energy transfer into the gas flow is due to convection with the glass cover.

But, for radiating gas, more energy transfer happens into gas flow by all heat transfer methods, including conduction, convection, and radiation that causes higher outlet temperature. The radiation heat transfer can be categorized into two parts; direct absorption of short wave incoming solar radiation and longwave radiation emitted by the hot surfaces. However, Fig. 13 shows a better performance for SGH due to the gas radiation effect because of more heat penetration from the absorber into the core of convective gas flow. This factor leads to a considerable decrease in the maximum heater temperature and resulted in less heat transfer irreversibility and prevented high exergy destruction and using thick insulations.
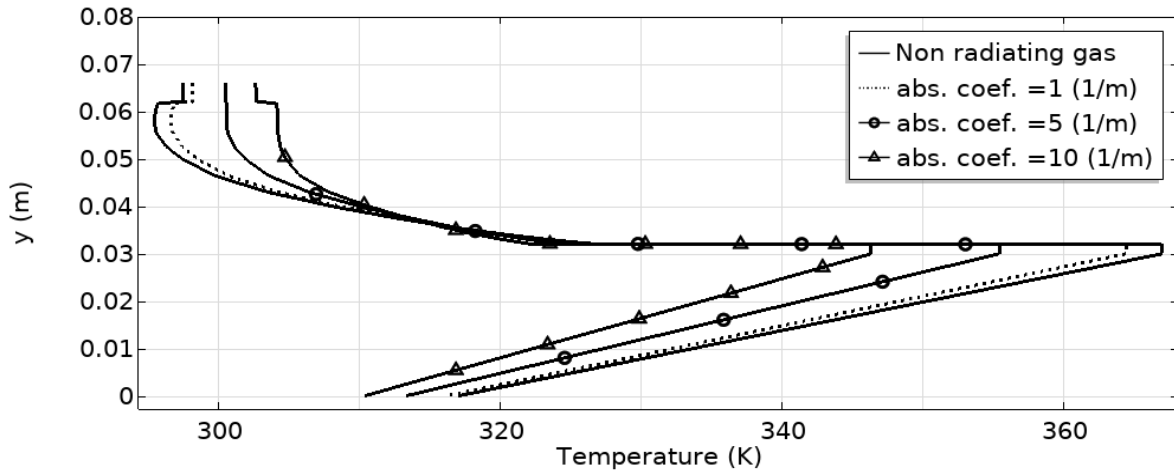
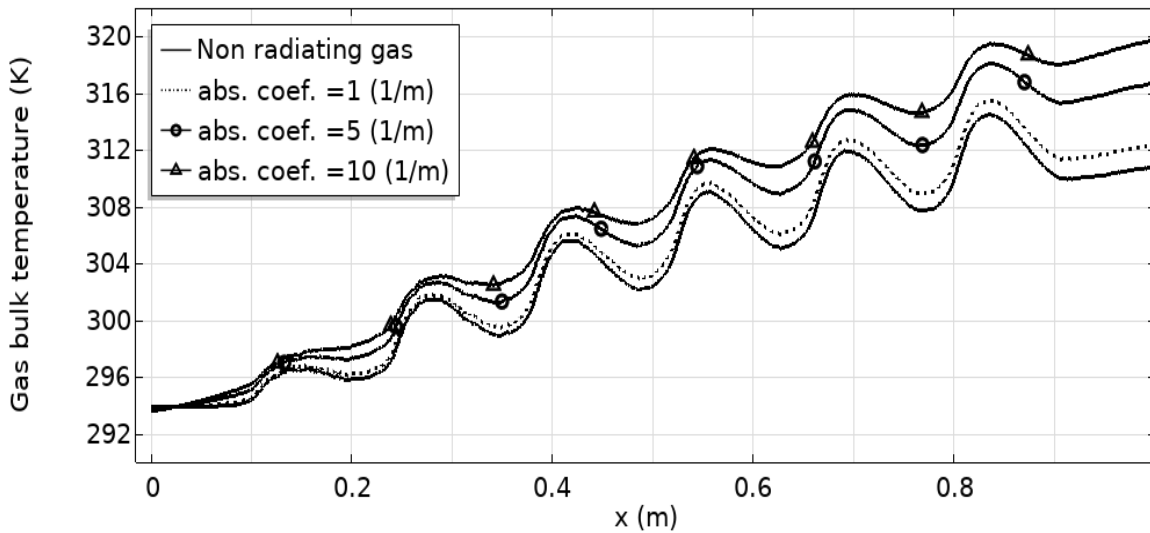**Fig. 13. Temperature distribution across the SGH at the midsection x=L/2**

Fig. 14. Gas mean bulk temperature distribution along the heater

The gas mean temperature distributions along the axial direction at different values of the radiative absorption coefficient, including the non-radiating case, are plotted in Fig. 14. The positive role of gas radiation effect on heat transfer enhancement is seen again. The higher gas outlet temperature is achieved for strongly radiative gas with $T_{m\,out} = 320$ K, while this temperature for non-radiating gas is 310 K. The wavy form of the gas temperature in the x-direction is due to the existence of ribs such that a higher rate of heat transfer from the absorber plate takes place in the vicinity of throating areas of the heater duct where the gas flow is accelerated.

The positive effect of gas radiation is also shown in Fig. 15, in which the variation of gas outlet temperature with absorption coefficient is plotted. This figure shows the higher

gas temperature at the outlet section in the case of using radiative working gas. As it is seen, the gas outlet temperature increases from $T_{out} = 310$ K for nonradiative gas to $T_{out} = 319$ K that happens for high radiative working gas with $\sigma_a = 10$ m^{-1}. It shows about a 60% increase in the amount of energy conversion from thermal radiation into gas enthalpy due to the gas radiation effect.

Since the energy loss from SAH takes place via the glass cover and insulation layer, the temperature distributions of these elements on their outer surfaces adjacent to the ambient are plotted in Fig. 16. As expected, both of these temperatures have an increasing trend along the x-direction, such that the gas radiation effect has two opposite effects on the temperature of these elements. As seen, the glass temperature in-
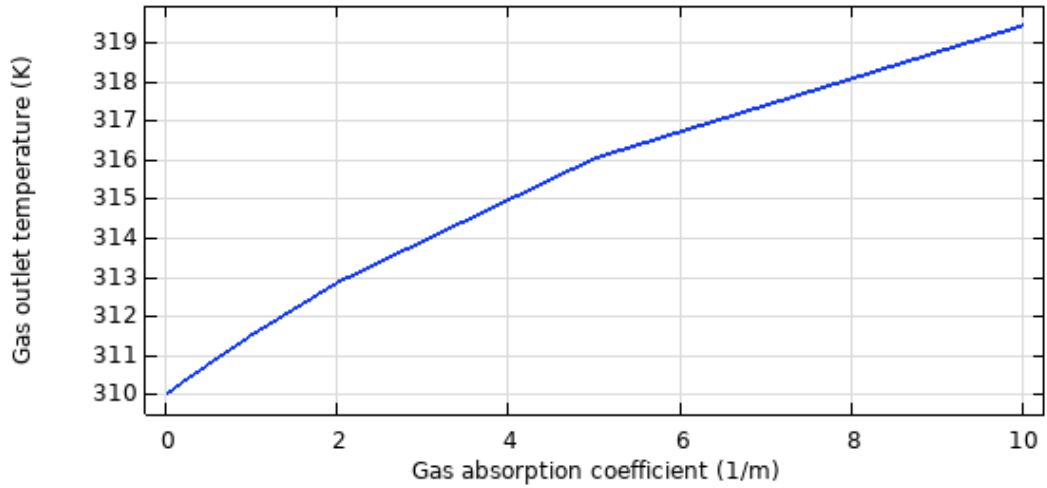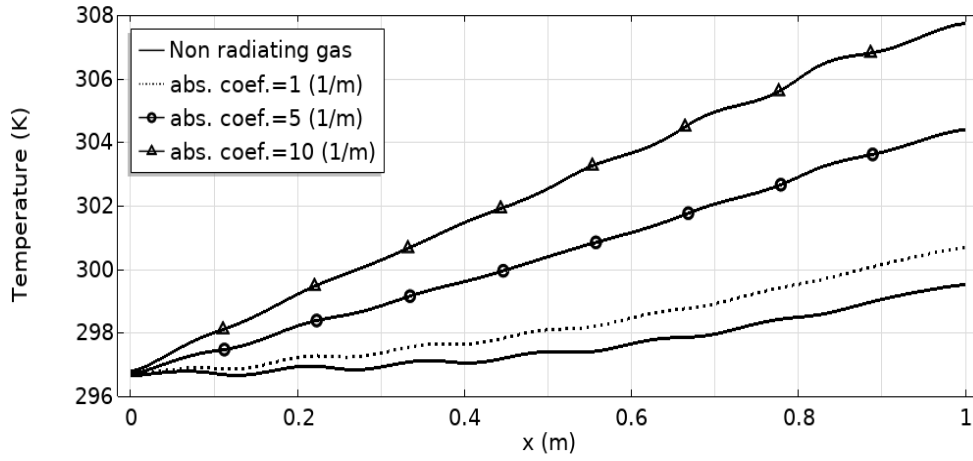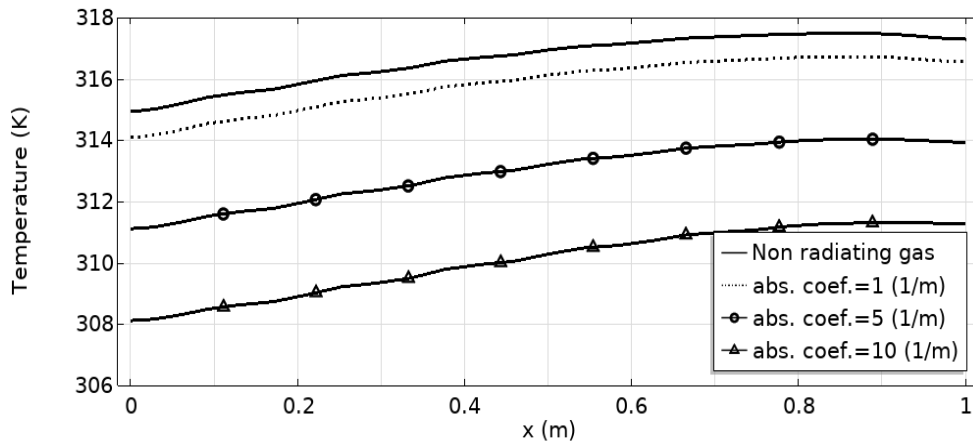
Fig. 15. Variation of outlet temperature with the gas absorption coefficient.

a)   Glass temperature

b)   Insulated temperature

Fig. 16. Distributions of the glass cover and insulation temperatures on their outer surfaces along the heater
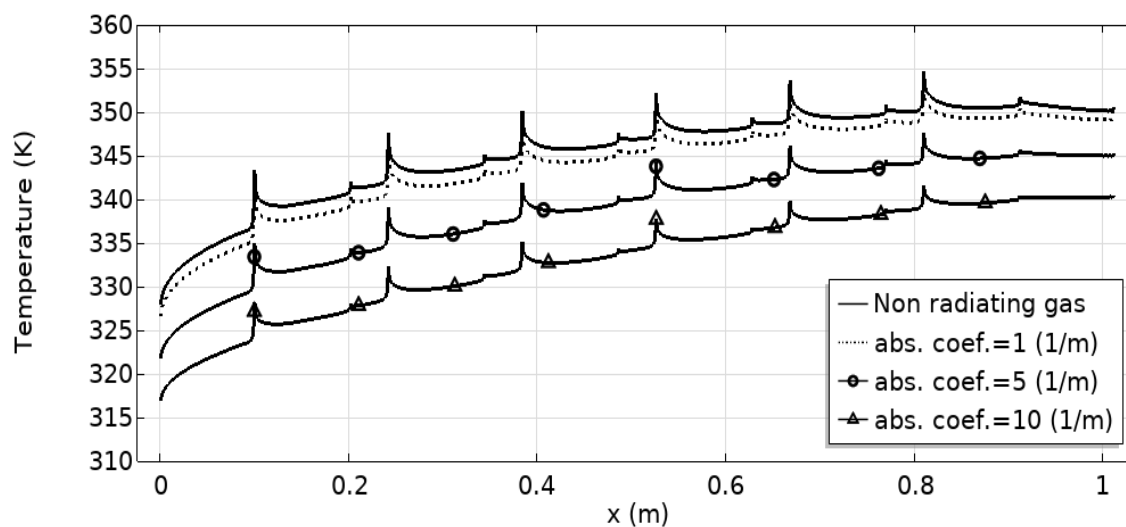
Fig. 17. Absorber surface temperature distribution in the axial direction

creases due to the gas radiation effect, and the opposite trend is seen for the temperature of the insulation layer. This is because the direct absorption of radiating gas and more heat transfer from the absorber surface into the convective flow causes a temperature decrease in the absorber plate and insulation layer. But as the temperature of radiating gas is higher than the non-radiating one, the glass cover which is in contact with the gas flow is affected and acts in the same manner.

In SGHs, the maximum temperature belongs to the absorber, which is an important part of these thermal systems. The temperature distributions along the surface of this element at different values of the gas absorption coefficient and for non-radiating gas are drawn in Fig. 17. The local jumps in temperature occur at the leading edge of ribs, where the working gas is stagnant. It is seen that the absorber temperature has an increasing trend along the flow direction, such that the minimum temperature of the absorber takes place for high radiating gas flow. As noted before, this behavior has a positive effect on the performance of SGH.

Up to this part of the paper, most of the findings were about the gas radiation effect. For illustrating the role of ribs and their airfoil-shaped geometry on heat transfer enhancement, the gas temperature contours in the clean SGH (without rib) are plotted in Fig. 18. If one compares this figure with Fig. 12, it can be found that more energy transfer from the absorber surface into convective gas flow occurs because of ribs. The ribs cause mixing in convection flow and breaking the thermal boundary layer and have the role of the extended surface. Both of these factors lead to heat transfer enhance-

ment and higher performance in SGHs. Otherwise, forming a thick thermal boundary layer in clean SGH in the absence of ribs decreases the heat transfer rate from the absorber into the gas flow. This factor also leads to considerable increases in the absorber and insulation temperatures, resulting in more energy loss from the SGH. If one compares the isotherm contours in Fig. 18 with each other, the positive effect of gas radiation on the heater's performance is still seen as it was observed before in the ribbed SGH.

One of the main reasons for choosing the airfoil-shaped rib in constructing a solar heater is its aerodynamic profile that leads to small pressure drops and pumping power. To verify this fact, the pressure variations along the centerline of the heater's duct in both clean and ribbed SGHs are drawn in Fig. 19 for comparison. The wavy form of pressure distribution due to the ribs was observed and discussed before in Figs. 9 and 10, but if one compares the pressure drop along with the heater for ribbed SGH ($(\Delta p = 0.68$ Pa) and clean SGH ($\Delta p = 0.4$ Pa), the low blockage effect of airfoil-shaped ribs can be seen.

To predict the thermal performance of SGH, thermal efficiency is defined to measure the heater's ability to convert solar irradiation into gas enthalpy as follows:

$$\eta = \frac{\dot{m}c_p(T_{mout} - T_{in}) - \dot{W}_{fan}}{q''_{sun}.A} \tag{21}$$

a) Non radiating gas

b) $\sigma_a = 1\ m^{-1}$

c) $\sigma_a = 5\ m^{-1}$

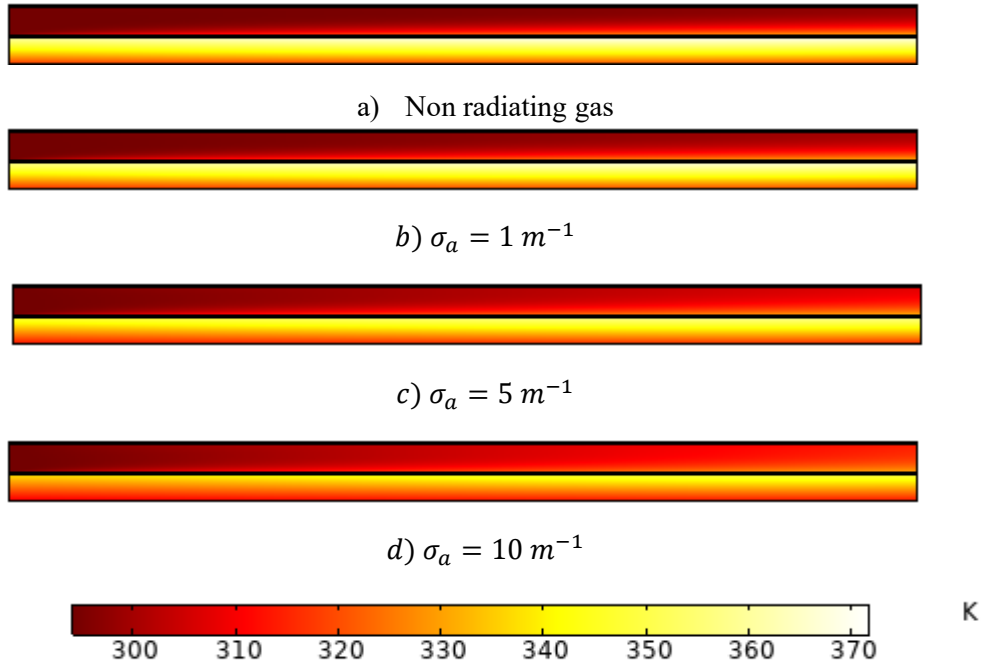d) $\sigma_a = 10\ m^{-1}$

K

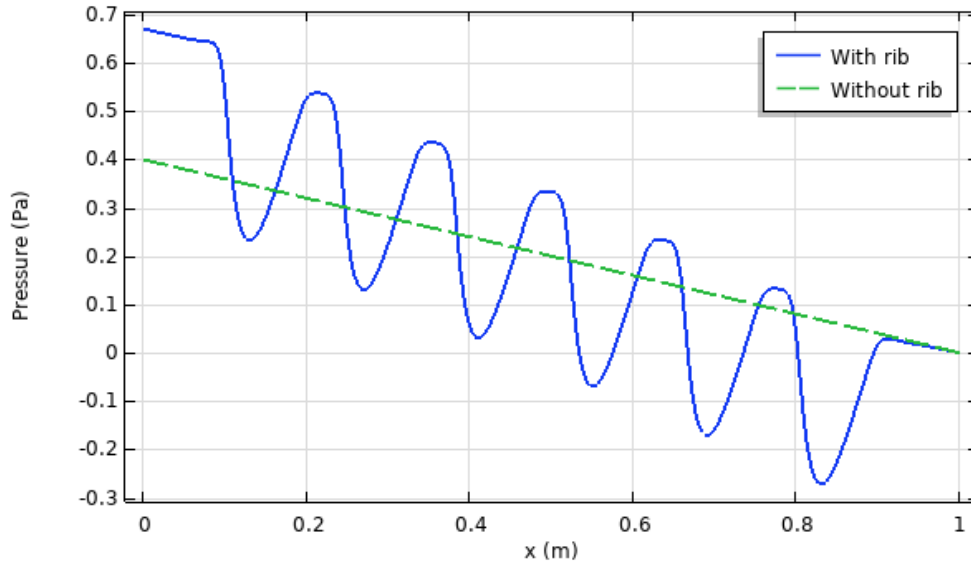**Fig. 18. Temperature contours inside the SGH**

Fig. 19. Gas pressure distributions along the centerline of SGHs with and without ribs
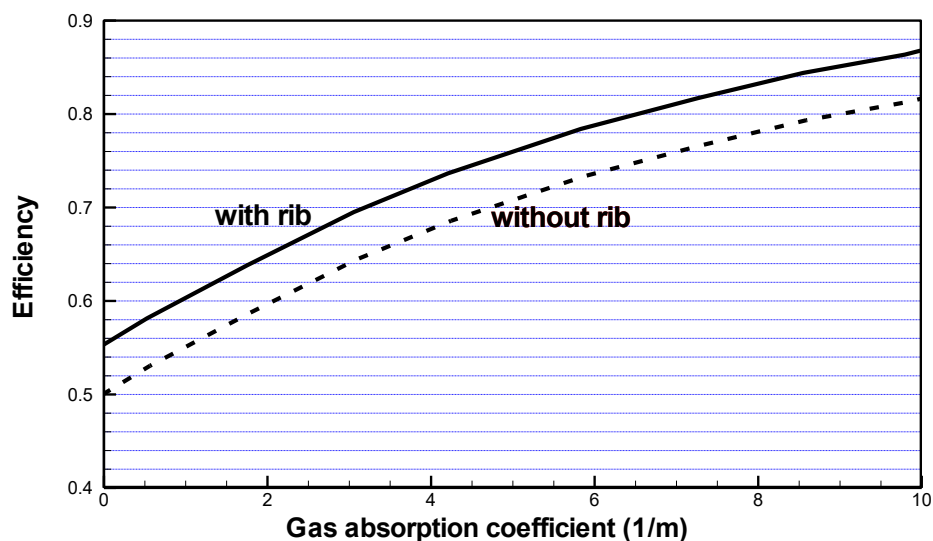
Fig. 20. Variations of thermal efficiency with gas absorption coefficient

In the definition of thermal efficiency, the pumping power ($\dot{W}_{fan} = \dot{m}\Delta p/\rho$), which is needed to compensate for the gas pressure drop along with the heater due to the friction loss, and also the ribs blockage effect is considered into account. In Fig. 20, the last figure, the thermal efficiency of SGH for both ribbed and clean heaters is quantitatively presented. At the same time, the radiative properties of working gas vary from weak ($\sigma_a = 0 \text{ m}^{-1}$) to strong ($\sigma_a = 10 \text{ m}^{-1}$) values. This figure illustrates the comparison between clean and ribbed SGHs at different values of the gas absorption coefficient. The increasing trend of the absorption coefficient for both types of heaters reveals the positive effect of gas radiation on the performance of energy conversion from solar radiation into gas enthalpy. This behavior was also seen in many previous figures. But, the main results that can be extracted from the curves in Fig. 20 are the positive effect of ribs in heat transfer enhancement and in increasing the thermal efficiency of SGH, especially under the presence of the gas radiation effect. Based on Fig. 20, about a 7% increase in thermal efficiency is seen because of the airfoil-shaped ribs. In addition, this type of rib causes a small pressure drop and low blockage effect with minimal intake pumping power. It can also be seen from Fig. 20 that the SGHs can reach the interesting maximum efficiency of 86% in the present test cases by simultaneous gas radiation and ribs effects, which makes the proposed SGH more efficient and productive.

5- Conclusion

This study was dedicated to a sustainable solution for the exploitation of renewable energy facilities through the thermal performance enhancement of SGHs by proposing the ra-diative gas and the airfoil-shaped ribs. After detailed thermo hydrodynamic analysis of extensive numerical experiments on the considered solar gas heater in steady-state turbulent forced convection regime with different amounts of gas absorption, peculiar and special characteristics of radiating gas is revealed under the presence of airfoil-shaped ribs. Through the presented results, radiative gases proved their full potential to serve as the future working gas in the solar gas heater. It also reveals its innate merit to be invested in SGHs application by showing magnificent 88% thermal efficiency because of simultaneous effects of gas radiation and airfoil-shaped ribs. Numerical findings show that for the normal test cases, equal to 66% increase in thermal efficiency is due to the gas radiation effect and a 7% increase by the attached ribs on the absorber surface, whose aerodynamic profiles cause a low blockage effect and provide minimal value for the pumping power. The present numerical findings reveal that, although most of the efficiency increase is due to the using participating gases in comparison to the ribs, but both of these factors are useful and cause an improvement in the performance of SGH.

Declaration of Competing Interest

The author declares that he has no known competing financial interests or personal relationships that could have appeared to influence the work reported in this paper.

Nomenclature

b	**Height of the air duct (m)**
C_p	Specific heat (kJ/kg K)
c	Airfoil chord (m)
D	Diameter (m)
h	Convection coefficient (W/m^{2}K)
k	Thermal conductivity (Wm^{-1}K^{-1})
L	Length of heater (mm)
G	Incident radiation (W/m^2. st)
I	Radiation intensity (W/m^2)
p	Pressure (Pa)
q	Heat flux (W/m^2)
Re	Reynolds number $= \frac{\rho \bar{V} D_h}{\mu}$
r	Position vector (m)
s	Radiation beam direction
T	Temperature (K)
V	Velocity (m/s)
(x, y)	Coordinates (m)

Subscript

b	black body
c	collimated
eq	equivalent
h	hydraulic
r	radiation
w	wall
t	**turbulent**
d	diffuse
m	bulk
amb	ambient

Greek symbols

α_{glass}	Glass absorptivity
ρ_{glass}	Glass reflectivity
τ_{glass}	Glass transmissivity
ϵ	Turbulent dissipation (m^2/s^3)
μ	Fluid Viscosity (Pa.s)
ρ	Fluid density (kg/m^3)
σ_s	Gas scattering coefficient (1/m)
σ_a	Gas absorption coefficient (1/m)
ε	Surface radiation emissivity
σ	Stefan–Boltzmann constant (W/m^{2}K^4)
Ω	Solid angle
κ	Turbulence kinetic energy (m^2/s^2)

Abbreviations

DOM	Discrete Ordinate Method
FEM	Finite element method
RTE	Radiative Transfer Equation
SAH	Solar Air Heater
SGH	Solar Gas Heater

References

[1] R. Gill, S. Singh, P.P. Singh, Low cost solar air heater, Energy Conversion and Management, 57 (2012) 131-142.

[2] A.D. Tuncer, A. Khanlari, A. Sözen, E.Y. Gürbüz, C. Şirin, A. Gungor, Energy-exergy and enviro-economic survey of solar air heaters with various air channel modifications, Renewable Energy, 160 (2020) 67-85.

[3] M. Aramesh, M. Ghalebani, A. Kasaeian, H. Zamani, G. Lorenzini, O. Mahian, S. Wongwises, A review of recent advances in solar cooking technology, Renewable Energy, 140 (2019) 419-435.

[4] S.A. Kalogirou, Solar thermal collectors and applications, Progress in energy and combustion science, 30(3) (2004) 231-295.

[5] A.E. Kabeel, M.H. Hamed, Z. Omara, A. Kandeal, Solar air heaters: Design configurations, improvement methods and applications–A detailed review, Renewable and Sustainable Energy Reviews, 70 (2017) 1189-1206.

[6] A.P. Singh, O. Singh, Thermo-hydraulic performance enhancement of convex-concave natural convection solar air heaters, Solar Energy, 183 (2019) 146-161.

[7] S. Singh, Experimental and numerical investigations of a single and double pass porous serpentine wavy wiremesh packed bed solar air heater, Renewable Energy, 145 (2020) 1361-1387.

[8] M. Nemś, J. Kasperski, Experimental investigation of concentrated solar air-heater with internal multiple-fin array, Renewable Energy, 97 (2016) 722-730.

[9] A.P. Singh, O. Singh, Curved vs. flat solar air heater: Performance evaluation under diverse environmental conditions, Renewable Energy, 145 (2020) 2056-2073.

[10] D. Jin, S. Quan, J. Zuo, S. Xu, Numerical investigation of heat transfer enhancement in a solar air heater roughened by multiple V-shaped ribs, Renewable energy, 134 (2019) 78-88.

[11] K. Nidhul, A.K. Yadav, S. Anish, S. Kumar, Critical review of ribbed solar air heater and performance evaluation of various V-rib configuration, Renewable and Sustainable Energy Reviews, 142 (2021) 110871.

[12] S.P. Shetty, N. Madhwesh, K.V. Karanth, Numerical analysis of a solar air heater with circular perforated absorber plate, Solar Energy, 215 (2021) 416-433.

[13] Y. Mahanand, J.R. Senapati, Thermo-hydraulic performance analysis of a solar air heater (SAH) with quarter-circular ribs on the absorber plate: A comparative study, International Journal of Thermal Sciences, 161 (2021) 106747.

[14] A. Dehghani Rayeni, S. Gandjalikhan Nassab, Effects of Gas Radiation on Thermal Performances of Single and Double Flow Plane Solar Heaters, International Journal of Engineering, 33(6) (2020) 1156-1166.

[15] M. Foruzan Nia, S.A. Gandjalikhan Nassab, A.B. Ansari, Numerical simulation of flow and thermal behavior of radiating gas flow in plane solar heaters, Journal of Thermal Science and Engineering Applications, 12(3) (2020) 031008.

[16] A.P. Singh, A. Kumar, O. Singh, Designs for high flow natural convection solar air heaters, Solar Energy, 193 (2019) 724-737.

[17] B.E. Launder, D.B. Spalding, The numerical computation of turbulent flows, in: Numerical prediction of flow, heat transfer, turbulence and combustion, Elsevier, 1983, pp. 96-116.

[18] M. Modest, Radiative Heat Transfer 2nd edn (New York: Academic), (2003).

[19] S. Singh, Performance evaluation of a novel solar air heater with arched absorber plate, Renewable Energy, 114 (2017) 879-886.

[20] A.B. Ansari, S. Nassab, Study of laminar forced convection of radiating gas over an inclined backward facing step under bleeding condition using the blocked-off method, Journal of heat transfer, 133(7) (2011).

[21] F. Chabane, N. Moummi, A. Brima, Experimental study of thermal efficiency of a solar air heater with an irregularity element on absorber plate, International Journal of Heat and Technology, 36 (2018) 855-860.

[22] F. Aissaoui, A.H. Benmachiche, A. Brima, D. Bahloul, Y. Belloufi, Experimental and theoretical analysis on thermal performance of the flat plate solar air collector, International Journal of Heat and Technology, 34(2) (2016) 213-220.